inventions

MDPI

Article

Load-Side Encoder-Based Redundant Control Framework for PMSG Wind Energy Conversion Systems

Zijian Zhang [1], Wenzhe Hao [1], Chao Luo [2], Jiawei Yu [2], Yihua Zhu [2], Zhiyong Dai [1] and Guangqi Li [1,*]

[1] School of Mechano-Electronic Engineering, Xidian University, Xi'an 710071, China; zijzhang@stu.xidian.edu.cn (Z.Z.); wenzhehao@stu.xidian.edu.cn (W.H.); zydai@xidian.edu.cn (Z.D.)
[2] State Key Laboratory of HVDC, Electric Power Research Institute, China Southern Power Grid, Guangzhou 510663, China; luochao@csg.cn (C.L.); yujw4@csg.cn (J.Y.); zhuyih@csg.cn (Y.Z.)
* Correspondence: gqli@xidian.edu.cn

Abstract

In permanent magnet synchronous generator-based wind energy conversion systems, generator-side measurements may become unreliable due to sensor faults, which can degrade system reliability. To address this issue, a redundant control framework based on load-side encoder feedback is proposed, where the load-side encoder serves as an alternative measurement source under sensor degradation. Compared with conventional generator-side sensing strategies, the proposed approach enhances fault tolerance without requiring additional hardware redundancy. An extended state observer is employed to estimate system states and lumped disturbances, enabling improved robustness. Simulation results show that the proposed method significantly improves speed tracking performance, reducing the root mean square error by approximately 45% compared with conventional PI control, while maintaining stable operation under sensor degradation conditions. The results demonstrate that the proposed strategy enhances system reliability and robustness in fault scenarios.

Keywords: permanent magnet synchronous generator; wind energy conversion system; load-side encoder; redundant control; extended state observer

1. Introduction

The increasing global demand for electricity and the urgent need to mitigate climate change pose significant challenges to traditional energy systems [1]. Globally, fossil fuels still dominate global electricity generation, accounting for approximately two-thirds of the total, and remain a major source of greenhouse gas emissions, contributing over 40% of energy-related CO_2 emissions [2]. This energy structure highlights the urgent need to accelerate the global transition toward low-carbon and sustainable energy systems [3,4]. In this context, renewable energy technologies have attracted increasing attention as effective solutions for reducing carbon emissions and improving energy sustainability. Emerging energy harvesting devices provide another route for sustainable energy generation and utilization [5]. Among various renewable energy sources, wind energy has attracted considerable attention due to its abundance, scalability, and technological maturity [6–8]. With continuous advancements and large-scale deployment, wind energy has become an important component of modern power systems and plays a key role in the global energy transition and new power system construction [9,10]. However, the increasing penetration of wind power also brings several challenges, such as intermittency, grid

Check for updates

Academic Editor: Eugen Rusu

Received: 15 April 2026
Revised: 9 May 2026
Accepted: 10 May 2026
Published: 15 May 2026

integration requirements, stability constraints, energy storage limitations, and system reliability issues [11,12]. These challenges place higher demands on wind energy conversion systems, requiring them to maintain efficient and stable operation under variable wind conditions and practical disturbances.

Against this background, modern renewable energy units, including wind energy conversion systems (WECSs), require advanced control strategies to ensure efficient and stable operation under varying operating conditions [13]. Techniques such as maximum power point tracking and pitch angle control are widely adopted to enhance system performance [14,15]. Among different generator configurations, permanent magnet synchronous generators (PMSGs) are commonly used due to their high efficiency and direct-drive capability [16]. However, PMSG-based systems are inherently nonlinear and subject to wind-speed fluctuations, disturbances, parameter uncertainties, and measurement issues [17,18]. In practical applications, reliable operation depends heavily on accurate speed and position measurements, which may degrade under harsh operating conditions [19]. These characteristics place higher demands on control strategies to ensure robustness and stability, particularly in the presence of measurement uncertainties and sensor faults.

To cope with nonlinear dynamics, disturbances, parameter uncertainties, and measurement uncertainties in PMSG-based systems, various control strategies have been investigated. Conventional proportional-integral (PI) control is widely used because of its simple structure and ease of implementation, but its performance strongly depends on accurate feedback measurements and proper parameter tuning. When the generator-side speed or position signal is affected by noise, bias, or degradation, PI control may suffer from increased tracking errors and speed fluctuations [20]. Advanced control strategies, such as sliding mode control (SMC) and model predictive control (MPC), have been developed to improve robustness and dynamic performance. However, SMC may introduce chattering and become sensitive to measurement noise under non-ideal sensing conditions [21,22], while MPC generally requires an accurate system model and reliable state measurements, with relatively high computational burden for real-time converter control [23,24]. Observer-based approaches, particularly extended state observer (ESO)-based methods, can estimate lumped disturbances and improve disturbance rejection without requiring a highly accurate mathematical model [25–28]. Nevertheless, most existing ESO-based methods still assume that the main feedback measurements are reliable. Therefore, although the above methods improve control robustness from different perspectives, they rarely address the measurement architecture itself, especially the utilization of redundant sensing information when generator-side measurements become degraded or unavailable. This limitation motivates the development of a redundant measurement-based control framework that can exploit load-side encoder feedback while compensating for the associated transmission dynamics, external disturbances, and measurement mismatch.

In this paper, a load-side encoder-based redundant control framework is proposed for PMSG-based WECSs under generator-side measurement degradation. In practical wind turbine applications, generator-side speed or position sensors may be affected by harsh environmental conditions, such as humidity, salt spray, temperature variations, and mechanical vibration, which can lead to measurement noise, signal degradation, or temporary sensor faults. To maintain continuous operation under such conditions, the load-side encoder is utilized as an alternative feedback source, thereby enabling fault-tolerant operation without adding extra hardware redundancy. However, the load-side measurement is not an ideal substitute for the generator-side measurement, because it may be affected by transmission dynamics, external disturbances, and measurement mismatch. Therefore, an extended state observer is integrated into the proposed framework to reconstruct system states and estimate lumped disturbances. Based on the estimated states and disturbances, a compensation mechanism is introduced to mitigate the influence of load-side measurement mismatch and external perturbations, improving system robustness under sensor degradation conditions. Simulation studies under various wind profiles, including step, ramp, and turbulent conditions, as well as parameter perturbations, demonstrate that the proposed framework achieves improved speed tracking performance and enhanced robustness compared with conventional control strategies.

The remainder of this paper is organized as follows. Section 2 presents the materials and methods, including the system model, ESO-based redundant control strategy, and stability analysis. Section 3 reports the simulation results. Section 4 discusses the validation scope and future extensions. Finally, Section 5 concludes the paper.

2. Materials and Methods

2.1. Modeling of PMSG-Based Wind Energy Conversion Systems

The wind energy conversion system can be described by standard aerodynamic and electromechanical models commonly used for PMSG-based wind-turbine analysis [29,30]. The captured wind power is given by

$$P = \frac{1}{2}\rho S C_p(\lambda) v_x^3 \tag{1}$$

where ρ, S, v_x, and C_p denote the air density, swept area, wind speed, and power coefficient, respectively.

The tip-speed ratio is expressed as

$$\lambda = \frac{\Omega_r R}{v_x} \tag{2}$$

and the aerodynamic torque is

$$T_a = \frac{P}{\Omega_r} \tag{3}$$

where Ω_r is the rotor speed and R is the blade radius.

The mechanical dynamics of the PMSG system can be described by

$$J\frac{d\omega_m}{dt} = T_L - T_e - B\omega_m + d \tag{4}$$

where J is the moment of inertia, ω_m is the mechanical angular speed, T_L is the load (driving) torque, T_e is the electromagnetic (braking) torque, B is the viscous friction coefficient, and d denotes external disturbances.

For a surface-mounted PMSG, the reluctance torque is neglected, and the electromagnetic torque is

$$T_e = \frac{3}{2} n_p \psi_f i_q \tag{5}$$

where n_p, ψ_f, and i_q are the number of pole pairs, permanent magnet flux linkage, and q-axis current, respectively.

Substituting (5) into (4) yields

$$\frac{d\omega_m}{dt} = b i_q + f \tag{6}$$

where

$$\begin{aligned} b &= -\frac{3}{2J} n_p \psi_f, \\ f &= \frac{1}{J} T_L - \frac{B}{J}\omega_m + \frac{d}{J}. \end{aligned} \tag{7}$$

https://doi.org/10.3390/inventions11030047

Here, f denotes the lumped disturbance, including aerodynamic torque variation, friction, and external disturbances. This compact form directly supports the ESO and disturbance compensation design.

2.2. ESO-Based Redundant Control for PMSG Systems with Load-Side Encoder

In the proposed redundant control framework, the load-side encoder is used as the alternative feedback source when generator-side measurements are degraded or unavailable. To handle transmission effects, model uncertainties, and external disturbances under this configuration, a disturbance estimation and compensation mechanism is introduced, as shown in Figure 1.

A third-order ESO is adopted to estimate the required states and lumped disturbance with relatively low model dependence and moderate implementation complexity. Other control formulations, such as robust control, sliding mode control, or model predictive control, may also be combined with the proposed load-side encoder feedback framework in future work.

The third-order nonlinear ESO with fal-based error feedback is designed as

$$\begin{aligned} \dot{\hat{\theta}}_m &= \hat{\omega}_m - \beta_1 fal(e, \alpha_1, \delta) \\ \dot{\hat{\omega}}_m &= bi_q + \hat{f} - \beta_2 fal(e, \alpha_2, \delta) \\ \dot{\hat{f}} &= -\beta_3 fal(e, \alpha_3, \delta) \end{aligned} \tag{8}$$

where the estimation error is defined as

$$e = \hat{\theta}_m - \theta_m \tag{9}$$

The nonlinear function $fal(\cdot)$ is defined as

$$fal(e, \alpha, \delta) = \begin{cases} \frac{e}{\delta^{1-\alpha}}, & |e| \leq \delta \\ |e|^{\alpha}\text{sign}(e), & |e| > \delta \end{cases} \tag{10}$$

where δ is a small positive constant that defines the boundary between the linear and nonlinear regions and balances noise sensitivity with convergence performance.

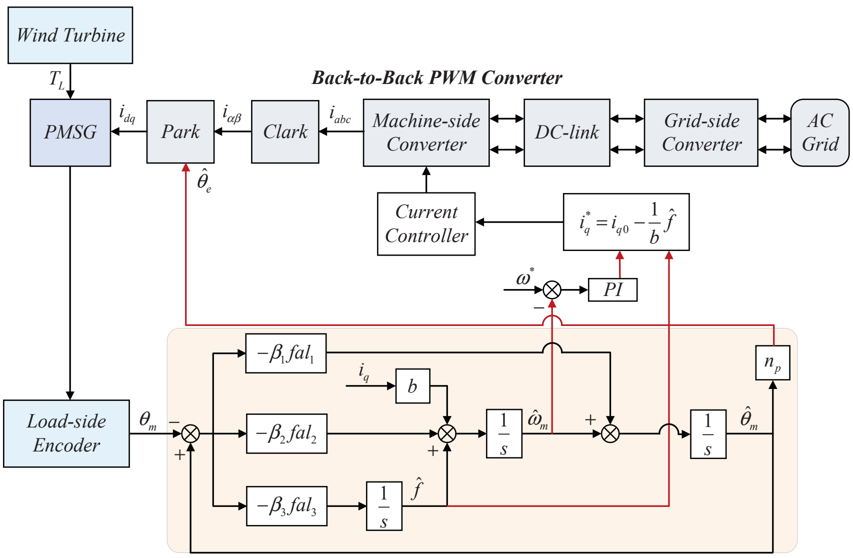

Figure 1. Block diagram of the proposed ESO-based redundant control framework for PMSG with load-side encoder configuration.

The observer gains β_1, β_2, and β_3 are initialized using the bandwidth parameterization method commonly adopted in ESO design. The basic idea is to first consider the local linearized error dynamics of the third-order ESO. When the estimation error is sufficiently small, the $fal(\cdot)$ function operates in its linear region and the observer error dynamics can be approximately represented by a third-order characteristic polynomial:

$$s^3 + \beta_1 s^2 + \beta_2 s + \beta_3 = 0. \tag{11}$$

To obtain a simple and tunable observer structure, the desired observer poles are assigned at $-\omega_o$, namely,

$$(s + \omega_o)^3 = s^3 + 3\omega_o s^2 + 3\omega_o^2 s + \omega_o^3. \tag{12}$$

By matching the coefficients, the observer gains are initialized as

$$\beta_1 = 3\omega_o, \quad \beta_2 = 3\omega_o^2, \quad \beta_3 = \omega_o^3 \tag{13}$$

where ω_o denotes the observer bandwidth.

In practical implementation, the observer bandwidth ω_o is not treated as an arbitrary parameter. It is first selected according to the bandwidth of the outer speed loop and the available measurement quality. In this work, ω_o is initialized as 3–5 times the closed-loop bandwidth of the speed controller. It is also kept lower than the bandwidth of the inner current loop and sufficiently below the sampling-frequency limit. Starting from this initial value, ω_o is increased until the estimated speed and disturbance converge sufficiently fast during wind-speed transients. If high-frequency oscillations, amplified encoder noise, or excessive current ripple appear, ω_o is reduced. The boundary parameter δ of the $fal(\cdot)$ function is also adjusted to enlarge the linear region. Therefore, the final observer gains are obtained through a practical trade-off among convergence speed, disturbance-estimation accuracy, noise sensitivity, and current smoothness.

However, improving estimation accuracy alone is not sufficient to eliminate the influence of disturbances and measurement uncertainties, especially under generator-side sensor degradation. To further enhance system reliability, the estimated disturbance is incorporated into the control law for active compensation. Let i_{q0} denote the nominal q-axis current command generated by the outer-loop speed controller without disturbance compensation. According to (6), the term bi_q represents the controllable part of the mechanical acceleration, whereas f represents the lumped disturbance. Therefore, by injecting the compensating current $-\hat{f}/b$, the final current reference applied to the current regulator is designed as

$$i_q^* = i_{q0} - \frac{\hat{f}}{b} \tag{14}$$

In the implementation, the control law uses the nominal input coefficient b, whose negative sign is determined by the generator torque convention in (4) and (5). Substituting (14) into (6) gives $\dot{\omega}_m = bi_{q0} + f - \hat{f}$, which indicates that the influence of the lumped disturbance can be reduced when $\hat{f}$ tracks f. Therefore, the compensation term is used to improve disturbance rejection based on the ESO estimate, while the robustness of the selected parameters under model perturbations is evaluated through the simulation cases.

2.3. Stability Analysis of the Proposed Method

In this section, the stability of the proposed ESO-based redundant control scheme is analyzed using Lyapunov stability theory. The load-side encoder is considered as the only measurement source, and the ESO is incorporated into the control framework to handle sensor uncertainties, disturbances, and potential generator-side measurement degradation. It will be shown that the estimation errors and tracking errors of the closed-loop system are uniformly ultimately bounded.

Define the observer estimation errors as

$$\begin{aligned} e_\theta &= \hat{\theta}_m - \theta_m \\ e_\omega &= \hat{\omega}_m - \omega_m \\ e_f &= \hat{f} - f \end{aligned} \tag{15}$$

According to the system dynamics and the ESO in (8), the error dynamics can be derived as

$$\begin{aligned} \dot{e}_\theta &= e_\omega - \beta_1 fal(e_\theta, \alpha_1, \delta) \\ \dot{e}_\omega &= e_f - \beta_2 fal(e_\theta, \alpha_2, \delta) \\ \dot{e}_f &= -\dot{f} - \beta_3 fal(e_\theta, \alpha_3, \delta) \end{aligned} \tag{16}$$

Consider the following Lyapunov candidate function:

$$V = \frac{1}{2}e_\theta^2 + \frac{1}{2}e_\omega^2 + \frac{1}{2}e_f^2 \tag{17}$$

Taking the time derivative of V yields

$$\begin{aligned} \dot{V} &= e_\theta \dot{e}_\theta + e_\omega \dot{e}_\omega + e_f \dot{e}_f \\ &= e_\theta e_\omega - \beta_1 e_\theta fal(e_\theta) \\ &\quad + e_\omega e_f - \beta_2 e_\omega fal(e_\theta) \\ &\quad - e_f \dot{f} - \beta_3 e_f fal(e_\theta) \end{aligned} \tag{18}$$

The lumped disturbance f represents the combined effect of model uncertainties, external disturbances (e.g., wind torque variations), and unmodeled dynamics. In practical wind energy systems, these disturbances vary with finite rates due to physical and mechanical constraints. Therefore, f and its derivative are assumed to be bounded, i.e.,

$$|\dot{f}| \le L \tag{19}$$

Then, using Young's inequality, the following inequalities hold:

$$\begin{aligned} e_\theta e_\omega &\le \frac{1}{2}e_\theta^2 + \frac{1}{2}e_\omega^2 \\ e_\omega e_f &\le \frac{1}{2}e_\omega^2 + \frac{1}{2}e_f^2 \\ e_f \dot{f} &\le \frac{1}{2}e_f^2 + \frac{1}{2}L^2 \end{aligned} \tag{20}$$

Substituting the above inequalities into $\dot{V}$ yields

$$\begin{aligned} \dot{V} \le \frac{1}{2}e_\theta^2 + e_\omega^2 + e_f^2 + \frac{1}{2}L^2 \\ - \beta_1 e_\theta fal(e_\theta) - \beta_2 e_\omega fal(e_\theta) - \beta_3 e_f fal(e_\theta) \end{aligned} \tag{21}$$

Define the error vector as $e = [e_\theta, e_\omega, e_f]^T$. By properly tuning the observer gains β_1, β_2, and β_3, the nonlinear feedback terms dominate the quadratic terms of the estimation errors. Therefore, $\dot{V}$ can be bounded as

$$\dot{V} \le -\lambda \|e\|^2 + C \tag{22}$$

where $\lambda > 0$ is a constant and $C = \frac{1}{2}L^2$.

Therefore, the estimation errors e_θ, e_ω, and e_f are uniformly ultimately bounded. Due to the disturbance compensation incorporated in the control law, the tracking error of the closed-loop system is also uniformly ultimately bounded. These results indicate that the proposed load-side encoder-based redundant control framework can maintain stable operation in the presence of disturbances, uncertainties, and generator-side sensor degradation.

3. Results

In this section, MATLAB/Simulink (R2023a) simulations are carried out to evaluate the proposed load-side encoder-based redundant control framework. The simulation model is established based on a 300 kW PMSG wind turbine system, and the key parameters are listed in Table 1. Four cases are considered under step, ramp, turbulent, and parameter-perturbed conditions, as summarized in Table 2. The dynamic responses of the proposed ESO-based method and the conventional PI controller are compared in the following figures.

The PI controller is selected as the baseline because it is widely used in practical wind energy conversion systems. The comparison is intended to evaluate the improvement brought by the proposed redundancy-and-compensation framework under the considered load-side encoder feedback configuration. More advanced controllers, such as SMC and MPC, may also be incorporated into the proposed framework and will be investigated in future work.

Table 1. Nominal Parameters of the PMSG Wind Turbine System.

Parameter	Symbol	Value
Moment of inertia (kg·m^2)	J	60
Viscous friction coefficient (N·m·s/rad)	B	0.078
Number of pole pairs	n_p	12
Permanent magnet flux (Wb)	ψ_f	3.88889
Stator resistance (Ω)	R_s	0.025
Stator inductance (mH)	L_m	3.6
Air density (kg·m^{-3})	ρ	1.2
Blade radius (m)	R	12
Rated wind speed (m/s)	v_r	4

Table 2. Simulation conditions.

Case	Wind Conditions
Case A	Step changes of wind speed.
Case B	Continuous ramp-up and ramp-down of wind speed.
Case C	Superimposed turbulent fluctuations of wind speed.
Case D	Continuous ramp-up and ramp-down of wind speed with a 20% increase in stator resistance and inductance of the PMSG.

Case A: Figures 2 and 3 illustrate the simulation results for Case A. Figure 2 contains two subplots, where the upper one illustrates the wind speed profile with step variations, and the lower one shows the corresponding power coefficient (C_p). It can be observed that C_p remains stable around 0.48, indicating effective maximum power point tracking. Figure 3 shows the rotor speed response and the corresponding tracking error for both the proposed ESO-based method and the conventional PI controller. Both methods are able to track the reference speed; however, the proposed method exhibits faster transient response and smaller tracking error, particularly during sudden wind speed changes. In addition, the RMSE of the proposed method is 0.9476, significantly lower than that of the PI controller (1.7650), which quantitatively confirms the improved tracking accuracy. These results indicate that the proposed method improves transient tracking performance under step wind conditions.

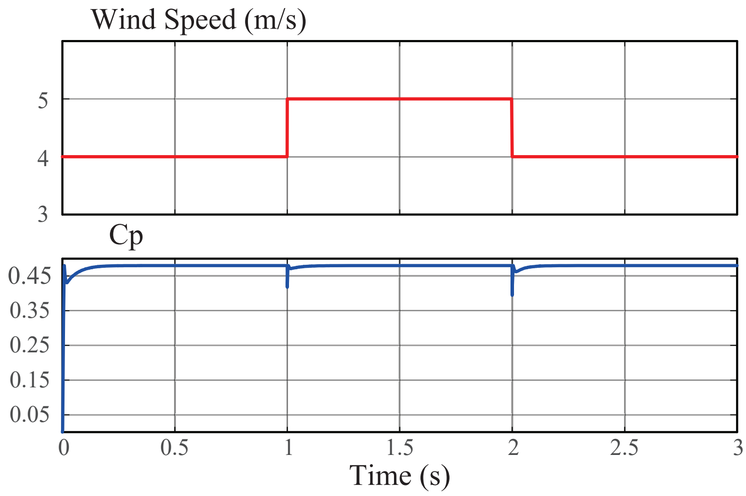

Figure 2. Simulation results for Case A: Wind speed and corresponding power coefficient C_p.

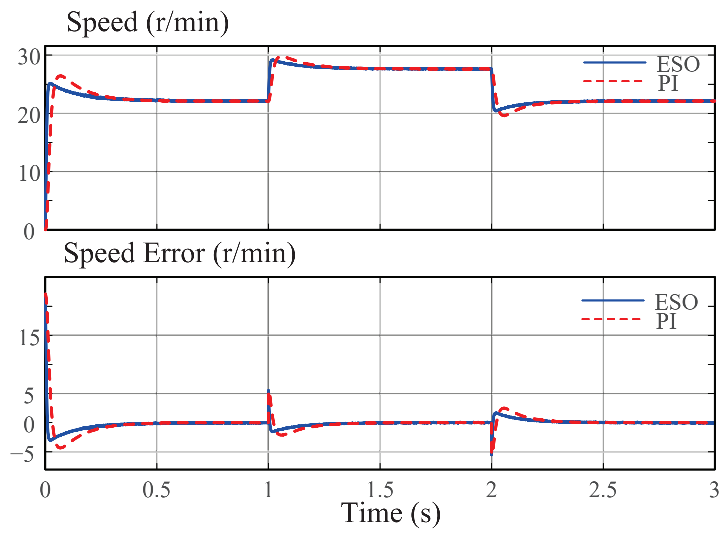

Figure 3. Simulation results for Case A: Speed response and speed error.

Case B: Figures 4 and 5 illustrate the simulation results under ramp wind conditions. As shown in Figure 4, the wind speed varies smoothly, and the corresponding power coefficient C_p remains close to 0.48 with only minor fluctuations, indicating stable maximum power point tracking performance. Figure 5 compares the rotor speed responses and tracking errors of the proposed ESO-based method and the conventional PI controller. Both methods achieve satisfactory tracking performance; however, the proposed method exhibits smaller tracking error throughout the process. The RMSE of the proposed method is 0.6546, which is lower than that of the PI controller (1.3417) and also smaller than that in Case A. This indicates that the proposed method maintains accurate tracking under smoother wind variation conditions.

Case C: Figures 6 and 7 illustrate the simulation results under turbulent wind conditions. As shown in Figure 6, the wind speed exhibits random and high-frequency fluctuations, resulting in noticeable variations in the power coefficient C_p, which remains close to its optimal operating range. Figure 7 compares the rotor speed responses and tracking errors of the proposed ESO-based method and the conventional PI controller. Under highly fluctuating wind conditions, both methods are able to follow the reference speed; however, the PI controller exhibits more pronounced oscillations, whereas the proposed method achieves smoother responses with reduced tracking error. The RMSE of the proposed method is 0.3414, which is significantly lower than that of the PI controller (0.6599). These results show that the proposed method maintains smoother speed tracking under turbulent wind conditions.

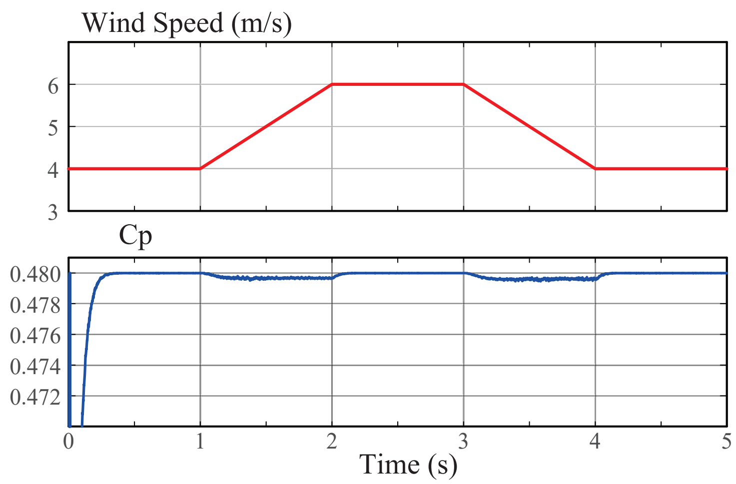

Figure 4. Simulation results for Case B: Wind speed and corresponding power coefficient C_p.

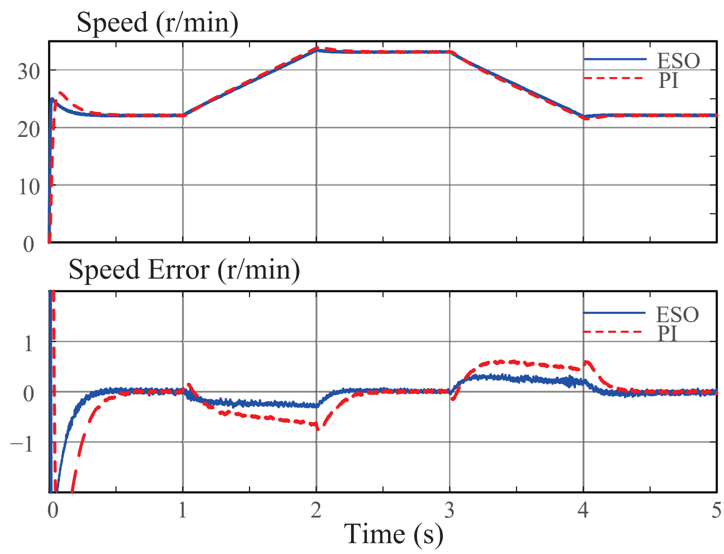

Figure 5. Simulation results for Case B: Speed response and speed error.

Case D: Figures 8 and 9 illustrate the simulation results under parameter uncertainty, where the stator resistance and inductance are increased by 20%. This case is introduced as a sensitivity test to examine whether the selected ESO gains and the proposed compensation strategy remain effective when the electrical parameters deviate from their nominal values. The same ramp wind profile as in Case B is applied for comparison. As shown in Figure 9, the rotor speed response of the proposed ESO-based method remains nearly unchanged compared to that in Case B, indicating that the tracking performance is only marginally affected by parameter variations. Quantitatively, the RMSE of the proposed method changes only from 0.6546 in Case B to 0.6583 in Case D, while the PI controller remains at a considerably larger error level. This small performance variation indicates that the ESO-based compensation remains effective under the 20% parameter perturbation. In contrast, parameter mismatches generally degrade control accuracy, especially for methods relying on nominal models. These results demonstrate that the proposed method exhibits robustness against parameter uncertainties, owing to the ESO-based compensation mechanism.

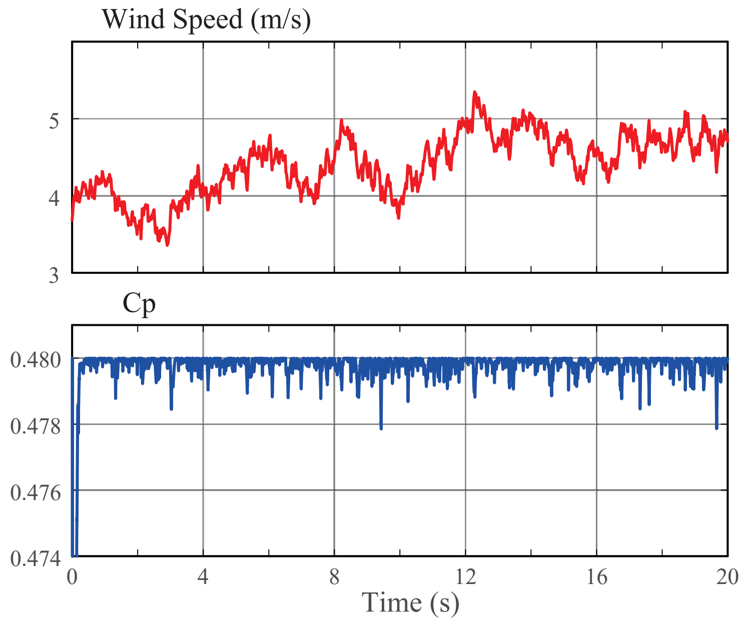

Figure 6. Simulation results for Case C: Wind speed and corresponding power coefficient C_p.

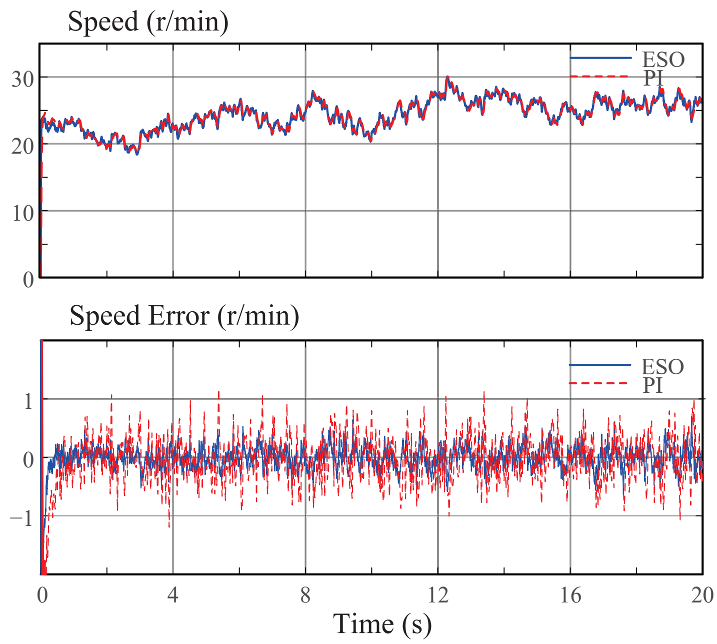

Figure 7. Simulation results for Case C: Speed response and speed error.

To quantitatively evaluate the tracking performance, the root mean square error (RMSE) of the speed is summarized in Table 3. The proposed ESO-based redundant control method with load-side encoder feedback consistently achieves lower RMSE values than the conventional PI controller. This confirms its improved tracking accuracy and robustness under different operating conditions.

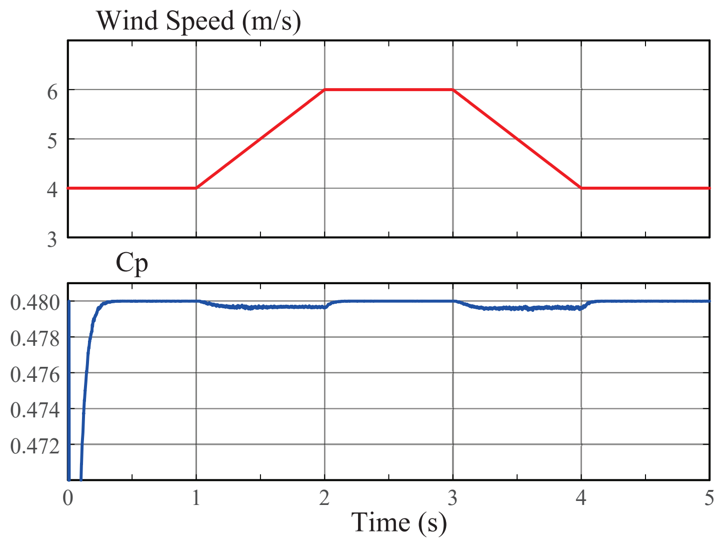

Figure 8. Simulation results for Case D: Wind speed and corresponding power coefficient C_p.

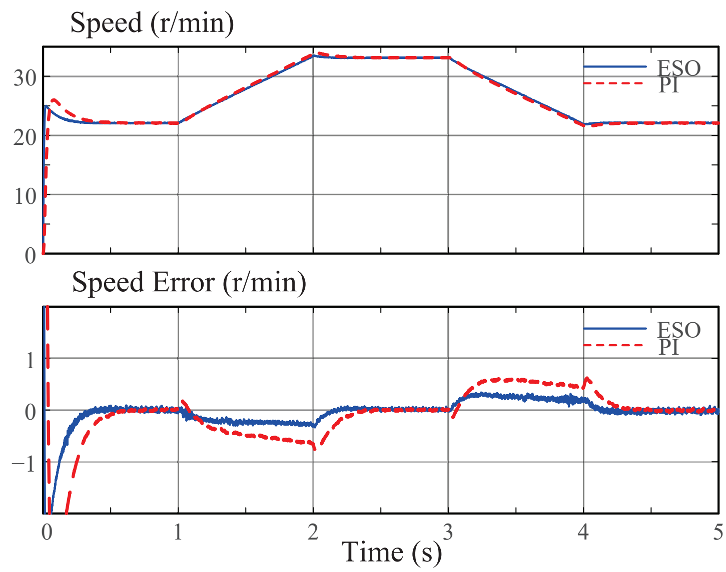

Figure 9. Simulation results for Case D: Speed response and speed error.

Table 3. RMSE comparison under different operating conditions.

Case	ESO RMSE	PI RMSE
Case A (Step)	0.9476	1.7650
Case B (Ramp)	0.6546	1.3417
Case C (Turbulent)	0.3414	0.6599
Case D (Param)	0.6583	1.3514

4. Discussion

The simulation results demonstrate that the proposed load-side encoder-based redundant control framework achieves improved tracking performance compared with the conventional PI controller, with reduced speed fluctuations and faster dynamic response. Moreover, the proposed method maintains stable operation under wind-speed variations and parameter perturbations. These results validate the effectiveness of the proposed framework for reliable operation under generator-side sensor degradation and system uncertainties.

The present simulations focus on validating the proposed redundant measurement framework and its ESO-based compensation realization. More advanced control strategies, such as SMC, MPC, and other ESO-based methods, can potentially be incorporated into the same load-side encoder feedback framework. Future work will compare these advanced controllers to further evaluate the generality and performance limits of the proposed framework.

5. Conclusions

This paper proposes a load-side encoder-based redundant control framework for PMSG-based wind energy conversion systems under generator-side measurement degradation. Different from conventional ESO-based or fault-tolerant control strategies, the proposed approach exploits the load-side encoder as an alternative measurement source, enabling continuous operation without relying on generator-side sensors. To address the challenges introduced by transmission dynamics and measurement mismatch, an ESO is integrated to reconstruct system states and estimate lumped disturbances, allowing accurate dynamic compensation under degraded measurement conditions.

Simulation results demonstrate that the proposed framework achieves improved tracking performance and effectively suppresses speed fluctuations compared with the conventional PI controller. Moreover, by combining measurement redundancy with disturbance estimation, the proposed framework enhances system robustness and ensures reliable operation under sensor degradation and parameter uncertainties, highlighting its potential for practical applications in wind energy conversion systems. Future work will investigate the integration of advanced control strategies, such as sliding mode control and model predictive control, into the proposed load-side encoder-based redundant framework. This will further evaluate its applicability under different measurement and operating conditions.

Author Contributions: Conceptualization, Z.Z. and W.H.; methodology, Z.Z. and W.H.; software, Z.Z.; validation, J.Y.; formal analysis, C.L.; writing—original draft preparation, Z.Z. and W.H.; writing—review and editing, Z.Z., J.Y. and C.L.; supervision, Z.Z. and Y.Z.; project administration, Z.Z. and G.L.; funding acquisition, Z.D. and J.Y. All authors have read and agreed to the published version of the manuscript.

Funding: This work was supported by the National Key Research and Development Program of China under Grant 2023YFB4203200, in part by Natural Science Foundation of Shaanxi Province 2025JC-YBMS-482.

Data Availability Statement: Data is contained within the article.

Conflicts of Interest: Authors Chao Luo, Jiawei Yu, and Yihua Zhu were employed by the company China Southern Power Grid. The authors declare that the research was conducted in the absence of any commercial or financial relationships that could be construed as a potential conflict of interest.

Abbreviations

The following abbreviations are used in this manuscript:

WECS	Wind Energy Conversion System
PMSG	Permanent Magnet Synchronous Generator
SMC	Sliding Mode Control
MPC	Model Predictive Control
ESO	Extended State Observer

References

1. Kumar, P.; Singh, O. Thermodynamic Analysis of Solid Oxide Fuel Cell–Gas Turbine–Organic Rankine Cycle Combined System. *Int. J. Mater. Sci. Mech. Eng.* **2019**, *6*, 98–102.
2. Ang, B.W.; Su, B. Carbon emission intensity in electricity production: A global analysis. *Energy Policy* **2016**, *94*, 56–63. [CrossRef]
3. Kumar, P.; Date, A.; Shabani, B. Techno-economic analysis of an integrated desalination–renewable–hydrogen system for zero-emission freshwater and electricity production. *Energy Convers. Manag.* **2026**, *353*, 121231. [CrossRef]
4. Tiismus, H.; Maask, V.; Astapov, V.; Korõtko, T.; Rosin, A. State-of-the-Art Review of Emerging Trends in Renewable Energy Generation Technologies. *IEEE Access* **2025**, *13*, 10820–10843. [CrossRef]
5. Zhang, J.-H.; Li, Y.; Du, J.; Hao, X.; Huang, H. A high-power wearable triboelectric nanogenerator prepared from self-assembled electrospun poly(vinylidene fluoride) fibers with a heart-like structure. *J. Mater. Chem. A* **2019**, *7*, 11724–11733. [CrossRef]
6. Tang, Z.; Yang, Y.; Blaabjerg, F. Power electronics: The enabling technology for renewable energy integration. *CSEE J. Power Energy Syst.* **2022**, *8*, 39–52.
7. Afridi, S.K.; Koondhar, M.A.; Jamali, M.I.; Alaas, Z.M.; Alsharif, M.H.; Kim, M.K.; Mahariq, I.; Touti, E.; Aoudia, M.; Ahmed, M.M. Winds of Progress: An In-Depth Exploration of Offshore, Floating, and Onshore Wind Turbines as Cornerstones for Sustainable Energy Generation and Environmental Stewardship. *IEEE Access* **2024**, *12*, 66147–66166. [CrossRef]
8. Rezwana, I.; Alam, S.M.S.; Hossain, E. Integrating Marine Hydrokinetic and Offshore Wind Energy: A Review of Technologies, Deployment, and Challenges. *IEEE Access* **2026**, *14*, 19996–20024. [CrossRef]
9. Kumar, P.; Paul, S.; Saha, A.K.; Yadav, O. Recent Advancements in Planning and Reliability Aspects of Large-Scale Deep Sea Offshore Wind Power Plants: A Review. *IEEE Access* **2025**, *13*, 3738–3767. [CrossRef]
10. He, Y.; Guan, L.; Wang, T.; Zhou, B.; Guo, Z.; Chen, H. Quantitative Evaluation and Analysis of Planning and Construction of the New Power System in China Southern Power Grid. *South. Power Syst. Technol.* **2024**, *18*, 40–53.
11. Zhang, J.; Liu, Y.; Qiu, J.; Liu, Z.; Yang, H.; Fu, C.; Li, S.; Zhu, Z.; Mao, Z. Transient Power Angle Stability Analysis of Regional New Energy Integration and Coordinated Control Strategy. *South. Power Syst. Technol.* **2024**, *18*, 129–138.
12. Chen, J.; Xiang, X.; He, Z.; Miao, Y. Reliability Assessment of Multi-State Unit Wind Farms Based on Improved Significant Sampling Methods. *South. Power Syst. Technol.* **2025**, 1–12. Available online: https://nfdwjs.csg.cn/gateway-web/en/debutDetail.html?serialNum=20241206004 (accessed on 26 March 2025).
13. Wu, Y.; Tang, Y.; Yu, Z.; Zhang, J. Online Adaptive Optimization Control Method for Renewable Energy Units Based on Dynamic Quantitative Assessment of Grid Stability. *South. Power Syst. Technol.* **2025**, 1–13. Available online: https://nfdwjs.csg.cn/gateway-web/en/debutDetail.html?serialNum=20250530002 (accessed on 28 December 2025).
14. Catalán, P.; Wang, Y.; Arza, J.; Chen, Z. A Comprehensive Overview of Power Converter Applied in High-Power Wind Turbine: Key Challenges and Potential Solutions. *IEEE Trans. Power Electron.* **2023**, *38*, 6169–6195. [CrossRef]
15. Hassan, A.; Ahmad, G.; Shafiullah, M.; Islam, A.; Alam, M.S. Review of the Intelligent Frameworks for Pitch Angle Control in Wind Turbines. *IEEE Access* **2025**, *13*, 29864–29885. [CrossRef]
16. Rolán, A.; Romero-Ramírez, E.; Bogarra, S.; Saura, J. Speed Estimation in PMSG-Based Wind Turbines From DC Voltage Measurement. *IEEE Trans. Instrum. Meas.* **2024**, *73*, 9005613. [CrossRef]
17. Wang, C.; Fan, Z.; Meng, J.; Sun, Y.; Zhou, Z.; Cui, J. Active Disturbance Rejection Control Strategy for Permanent Magnet Synchronous Wind Power System. In *Proceedings of 2023 8th Asia Conference on Power and Electrical Engineering (ACPEE)*; IEEE: New York, NY, USA, 2023; pp. 811–815.
18. Aguilar-Orduña, M.; Sira-Ramírez, H.; Gómez-León, B.C. On the Active Disturbance Rejection Control for the sensorless Maximum Power Point Tracking task of a variable speed wind turbine. In *Proceedings of the 2022 IEEE 61st Conference on Decision and Control (CDC)*; IEEE: New York, NY, USA, 2022; pp. 3164–3169.
19. Zhao, Y.; Wei, C.; Zhang, Z.; Qiao, W. A Review on Position/Speed Sensorless Control for Permanent-Magnet Synchronous Machine-Based Wind Energy Conversion Systems. *IEEE J. Emerg. Sel. Top. Power Electron.* **2013**, *1*, 203–216. [CrossRef]
20. Kumar, A.; Prakash, S.; Ghosh, S.; Naidu, N.S.; Dworak, P. Robust Decentralized PI Controller Design for Permanent Magnet Synchronous Generator. *IEEE Open J. Ind. Electron. Soc.* **2025**, *6*, 1617–1628. [CrossRef]
21. Wei, C.; Yin, T.; Qiao, W.; Zhu, Y. Disturbance Rejection Control for PMSGs Based on Novel Sliding Mode Control Law and Unknown System Disturbance Estimator. *IEEE Trans. Energy Convers.* **2025**, *40*, 3142–3151. [CrossRef]
22. Abu-Askar, A.; Gulzar, M.M.; Khalid, M. A Novel Approach for Wind Turbine Robust Speed Control Using Sliding Mode Control with Extended State Observer. In *Proceedings of 2023 IEEE IAS Global Conference on Renewable Energy and Hydrogen Technologies (GlobConHT)*; IEEE: New York, NY, USA, 2023; pp. 1–7.
23. Basheer, A.A.; Jeong, J.H.; Lee, S.R.; Joo, Y.H. Power Maximization Using Finite-Control-Set Model Predictive Control Strategy for Wind Turbine Systems. *IEEE J. Emerg. Sel. Top. Ind. Electron.* **2025**, *6*, 238–247. [CrossRef]
24. Li, J.; Babayomi, O.; Zhang, Z.; Li, Z. Robust Predictive Current Control of PMSG Wind Turbines with Sensor Noise Suppression. *Energies* **2023**, *16*, 6255. [CrossRef]

25. Lin, P.; Zhang, S.; Wu, Z.; Li, J.; Sun, X.M. A Linear–Nonlinear Switching Active Disturbance Rejection Voltage Controller of PMSG. *IEEE Trans. Transp. Electr.* **2022**, *8*, 3367–3378. [CrossRef]
26. Li, G.; Guo, R.; Chen, J.; Liu, X. A Single-Loop Active Disturbance Rejection Control of PMSG for Suppressing Subsynchronous Resonance. *IEEE Trans. Ind. Electron.* **2025**, *72*, 10233–10242. [CrossRef]
27. Yang, G.; Chen, L.; Cai, P.; Gao, W.; Ai, C. Adaptive Disturbance Rejection and Power Smoothing Control for Offshore Hydraulic Wind Turbines Based on Pitch and Motor Tilt Angles. *Energies* **2024**, *17*, 6244. [CrossRef]
28. Zhao, J.; Li, R.; Wang, H.; Jiang, J.; Hu, B. Deadbeat Predictive Current Control for CMG Ultra-Low Speed PMSM Emulator Based on Cascaded Extended State Observer. *Electronics* **2026**, *15*, 1527. [CrossRef]
29. Perera, S.M.H.D.; Putrus, G.; Conlon, M.; Narayana, M.; Sunderl, K. Wind Energy Harvesting and Conversion Systems: A Technical Review. *Energies* **2022**, *15*, 9299. [CrossRef]
30. Orlando, N.A.; Liserre, M.; Mastromauro, R.A.; Dell'Aquila, A. A Survey of Control Issues in PMSG-Based Small Wind-Turbine Systems. *IEEE Trans. Ind. Inform.* **2013**, *9*, 1211–1221. [CrossRef]